Avalanche photodiode based detector for beam emission spectroscopy

D. Dunai,[1] S. Zoletnik,[1] J. Sárközi,[1] and A. R. Field[2]
[1]*KFKI Research Institute for Particle and Nuclear Physics, EURATOM Association, P.O. Box 49, H-1525 Budapest, Hungary*
[2]*EURATOM/CCFE Fusion Association, Culham Science Centre, Abingdon, Oxon OX14 3DB, United Kingdom*

(Received 12 October 2009; accepted 20 August 2010; published online 20 October 2010)

An avalanche photodiode based (APD) detector for the visible wavelength range was developed for low light level, high frequency beam emission spectroscopy (BES) experiments in fusion plasmas. This solid state detector has higher quantum efficiency than photomultiplier tubes, and unlike normal photodiodes, it has internal gain. This paper describes the developed detector as well as the noise model of the electronic circuit. By understanding the noise sources and the amplification process, the optimal amplifier and APD reverse voltage setting can be determined, where the signal-to-noise ratio is the highest for a given photon flux. The calculations are compared to the absolute calibration results of the implemented circuit. It was found that for a certain photon flux range, relevant for BES measurements ($\approx 10^8-10^{10}$ photons/s), the new detector is superior to both photomultipliers and photodiodes, although it does not require cryogenic cooling of any component. The position of this photon flux window sensitively depends on the parameters of the actual experimental implementation (desired bandwidth, detector size, etc.) Several detector units based on these developments have been built and installed in various tokamaks. Some illustrative results are presented from the 8-channel trial BES system installed at Mega-Ampere Spherical Tokamak (MAST) and the 16-channel BES system installed at the Torus Experiment for Technology Oriented Research (TEXTOR). © *2010 American Institute of Physics.* [doi:10.1063/1.3488458]

I. INTRODUCTION

Understanding the physics of plasma turbulence in fusion experiments is one of the key issues in magnetic fusion research. Turbulence theories need to be cross-checked against experiments; therefore, the past decades have seen a continuous development for more effective fluctuation measurements. Beam emission spectroscopy (BES) is one of the widely used techniques.[1] The phrase covers a collection of methods sharing the same basic idea: a beam of neutral atoms penetrates the plasma and the particles are collisionally excited by the plasma species. The light emitted from the radiative decay of one or more atomic transitions is collected, which contains information on the local plasma density and sometimes temperature. Fluctuation in the plasma density and the temperature causes fluctuation in the light emission; therefore, BES is an excellent technique for local fluctuation measurement, where localization comes from the intersection of the beam and the optical sightline. BES implementations differ in the beam species; alkali beams (lithium or sodium) or He gas jets can be used for diagnosing the plasma edge, while heating hydrogen (deuterium) beams can be applied in the plasma core measurements. Different multichannel schemes have been developed,[2,3] providing two-dimensional (2D) measurements, which give an extremely detailed insight into the spatiotemporal structure of turbulence.

Careful modeling of the beam plasma interaction and the synthetic diagnostics, i.e., a numerical model of the measurement, are needed to find optimum solutions for each component of the experiment. In realistic situations, such models predict 10^8-10^{12} photons/s on the detector of one measurement channel. The desirable frequency range of the fluctuation measurement extends to about 1 MHz, resulting in photon statistical noise level (the square root of the number of detected photons during the integration time of the detector) at 0.1%–10% of the signal. This is exactly the range of the expected density fluctuation level at the plasma edge (10%) and core (0.1%);[4] therefore, an optimum light detector is needed where the signal-to-noise ratio approaches the above theoretical limit. It has to be noted that a similar study has been published in literature more than 15 years ago.[5] Since that time, avalanche photodiode (APD) detector and amplifier technology have been developed, considerably justifying new development work.

The aim of the work presented in this paper was to find the optimum detector solution for three BES experiments: (1) a core BES system using a heating beam at the Mega-Ampere Spherical Tokamak (MAST); (2) a fast observation system for the accelerated lithium beam diagnostic of the Joint European Torus (JET); and (3) a fast observation system for the Torus Experiment for Technology Oriented Research (TEXTOR) 35 keV accelerated lithium beam. From the point of view of the key parameters of the detector selection, these systems are similar: 1–2 MHz bandwidth and 10^9-10^{11} photons/s.

This paper is organized as follows. In Sec. II, an overview of detector options is given. Based on the overview, an APD detector is selected. Section III describes the electronics circuit. The noise model is presented in Sec. IV and is compared to measurements. Some illustrative BES results are shown in Sec. V.

II. OVERVIEW OF DETECTOR OPTIONS

In this section, we compare the properties of the three widely used detector options: the photomultiplier tube (PMT), the APD, and the photoconductive photodiode (PPD). We will compare these detectors from the point of view of the attainable signal-to-noise ratio (SNR) as a function of incoming photon flux. The SNR is the key parameter in a BES experiment since it defines what could be deduced from the measured signals. The maximum theoretically achievable SNR of the detector is limited by the photon statistical noise. The origin of this noise is the finite number of the detected photons. As we aim at detecting the relative fluctuations in the light source below 10%, we do not count photons but detect the light level with a given bandwidth (B). Photon emission from a stable light source follows a Poisson distribution because the emission of the photons is an instantaneous and independent event. From the detected photon flux Φ, the detector finite bandwidth integrates $N = \Phi / 2\pi B$ photons. If $N \gg 1$, the signal will follow normal distribution and the SNR from the relative photon statistical noise becomes $\mathrm{SNR}_{\mathrm{photon}} = \sqrt{\Phi / 2\pi B}$. The aim is to keep the noise level close to this theoretical limit, which means as many emitted photons as possible has to be collected while keeping the noise of the detection and amplification process low. The collection solid angle is limited by the spatial resolution and by other geometrical constraints; therefore, a high quantum efficiency (QE) detector is essential. Although the QE of the detector is dependent on the wavelength of the radiation in the target experiments mentioned above, we aim at measuring either the 656.1 nm D^0 or the 670.8 nm lithium 2p-2s transition; therefore, we are looking at nearly the same wavelength and we do not consider the wavelength dependency of the QE.

PMTs have been used widely in various BES experiments, e.g., Wendelstein 7-AS (Ref. 6) and Axially Symmetric Divertor Experiment (ASDEX) Upgrade.[7] They have a high (up to 10^7) and relatively low noise intrinsic gain, which results in a high (from microamperes to milliamperes) output signal. The measured signal usually does not need special amplifier electronics or even can be directly digitized. This means that the S/N level is very close to the photon statistical limit calculated with the detected photon flux. The PMT's disadvantage is the low QE. Even using the most advanced multialkali photocathodes, it is around 10%, which means about a factor of 3 lower SNR than the theoretical maximum. PMTs are additionally very sensitive to magnetic field, which complicates their use close to the magnetic fusion device. The solution can be magnetic shielding, which is not desirable close to the machine since it can modify the field. Optical fibers can be used to move the detectors away from the device and couple the light of the individual detectors. Coupling and fiber attenuation are additional sources of light loss and the cost can be considerable.

At TFTR and later at DIII-D,[2] a different solution was developed, where PPDs have been used from 1992 with excellent results. When a photon with energy above the gap energy strikes the photodiode, an electron inside the crystal structure is moved to the conduction band, leaving a hole in the valence band. When voltage is applied to the photodiode, these electrons and holes generate a current flow. The main advantage of using solid state detectors is the high QE, which, in the 650–670 nm region, is as high as 80%–85%. The PPDs do not have intrinsic gain; therefore, even at a quite high photon flux, their signal is very low (10^{10} photons/s ~ 1.5 nA). This requires a state-of-the-art amplifier and read out electronics. Even the newest fast field-effect transistor (FET) input operational amplifiers combined with a load resistor are unacceptably noisy at room temperature. To decrease the noise level and the dark current, the first stage of the amplifier with the diode can be cryogenically cooled. A cryogenically cooled observation system makes the direct imaging difficult. Fibers have to be used, which can be expensive in a multichord measurement.

In the PPD system at low light level, the detector and amplifier noise has a fixed amplitude and dominates the noise; therefore, in this range, the SNR will change with the signal level and not with its square root. At some light level, the photon statistical noise overcomes this fixed noise and the detector will work very close to the photon statistical limit. For high photon flux applications where the generated current can be amplified effectively, the PPDs represent the ideal solution. Additionally, solid state detectors are less sensitive to magnetic fields; therefore, compact high resolution detectors can be built such as photodiode line sensors or complementary metal-oxide semiconductor (CMOS) image sensors close to a fusion device.

There is a gap in the applications between PPDs and PMTs where APDs can be the best choice. This type of detector has also been used for BES measurements.[8] APDs are photodiodes utilizing an internal gain mechanism that functions by applying a high reverse voltage (in the few hundred volt range) and operating the device in the breakdown range. In a low light level measurement where the read out noise dominates, using a PPD, the internal gain of the APD can improve the detection limit with the factor of the intrinsic gain. The QEs of the up-to-date APDs are similarly high, $\sim$80%–85%, like the PPDs. The APD multiplication process contains statistical fluctuations, as the electron avalanche development is a statistical process on its own. This "excess noise" causes a somewhat higher fluctuation in the detector output current for the APD than for a PPD. Since it is statistically indistinguishable from the photon noise, it can be expressed as a reduction of the effective QE. As the excess noise increases with the detector bias voltage (gain), it is not optimal to use the highest available gain, but increase the voltage only to the point where the photon statistical noise overcomes the amplifier noise. This setting typically results in an effective QE of 30%–45%, but nevertheless, in a certain photon flux range, the SNR of the APD will be higher than that of the PPD.

The gain of the APD and the dark current also shows temperature dependence; therefore, the APDs should be temperature stabilized but they do not need to be operated at

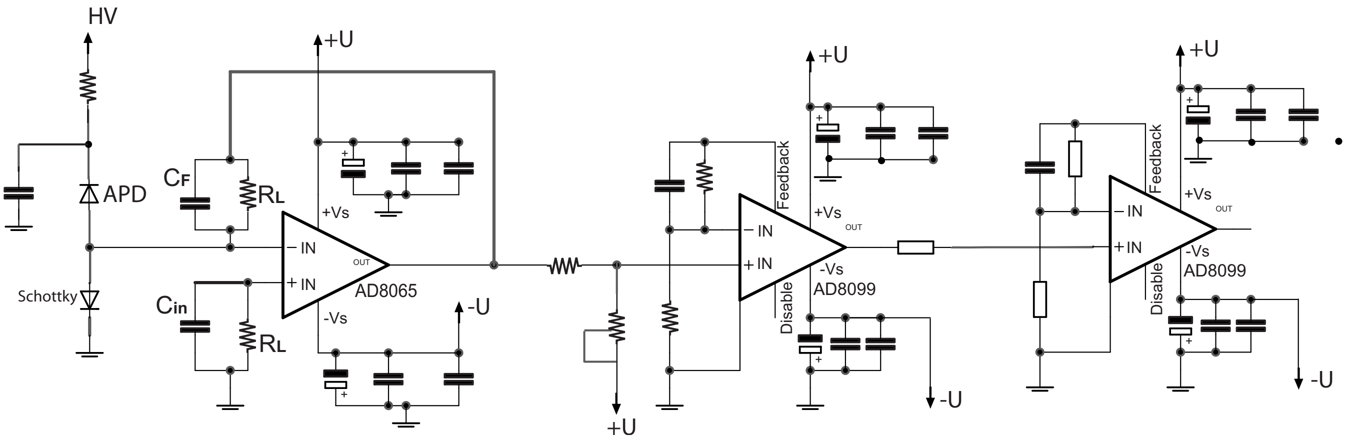

FIG. 1. Schematic of the electronics.

cryogenic temperatures. As a recent development, the photon counting APD technology should also be mentioned. In this case, the detectors are operated in a so-called Geiger mode, when an incoming photon completely breaks down the diode. If the diode is driven through a high-enough resistance, the current is limited and the diode is not damaged. The gain of the APD in this mode of operation is in the 10^5 range; therefore, the individual photons produce a well measurable pulse, but, of course, the detector will not be sensitive to more photons during the recovery time. By manufacturing an array of small diodes on a single substrate and adding their output current, one gets a compact solid state detector with photon counting capability in the $10^8 - 10^{10}$ photons/s range. Although in the long run this technology might provide both the PMT and APD capabilities, its peak QE is presently limited to about 50%. Around 650 nm, the QE is close to 20%; therefore, it is not considered in this paper.

III. ELECTRONIC CIRCUIT

The desired bandwidth of the detector system is chosen to be 1 MHz and the estimated photon flux varied widely between plasma configurations on different devices and measurement channels, but roughly between 10^8 and 10^{11} photons/s. In this section, we consider the properties of a generic low noise amplifier circuit, calculate the achievable S/N ratio for APD and PPD detectors, and compare them with each other and also with PMT.

The electronic circuit is shown in Fig. 1. The schematic can be functionally divided into three parts: the APD detector with its protecting elements, the current to voltage converter (left operational amplifier), and the amplifier stage consisting of two amplifiers.

The APD is protected by a series of resistors that limit the detector current in case of a too high incoming light level. A series of capacitors filters the shot noise of these resistors, providing a fixed input bias voltage. A fast Schottky diode prevents the input of the first stage amplifier being raised to high voltage. This proved to be essential to protect the first stage amplifier.

The key component of the circuit is the first stage current to voltage converter, also known as the preamplifier. After a detailed survey of several possibilities, the AD8065 ultralow noise, high bandwidth FET input operational amplifier was chosen. It has extremely low input voltage and current noise figure ($7\ \mathrm{nV}/\sqrt{\mathrm{Hz}}$ and $0.6\ \mathrm{fA}/\sqrt{\mathrm{Hz}}$, respectively) and 145 MHz bandwidth (-3 dB point).[9] It also has a low input bias current, therefore provides a stable offset.

The amplifier stage consists of two high performance low noise high gain bandwidth product AD8099 operational amplifiers (3.8 GHz at 3 dB with unity gain). They are typically set to operate with a combined gain of ~ 100. The last amplifier also acts as a line driver, enabling the digitizers to be placed at a distance.

The supply voltages of all amplifier stages are carefully filtered. An offset adjustment potentiometer is added between the current-to-voltage converter and the second stage, as it was experienced that the system can have a significant offset that changes from channel to channel. This is caused by the amplifier offset and not by the dark current of the detector. In some applications, this manual offset null capability was replaced by a computer controlled dc analog input produced by a digital to analog converter.

The detector electronics was built using surface mount device technology to keep the parasitic capacitances minimal and the size small. It was found to be beneficial to separate the grounds of the individual channels and connect them only at the output. The resistor and capacitor values of the first stage are determined using noise analysis in Sec. IV.

IV. SIMULATION OF NOISE FIGURES

To make a proper simulation of the noise figure of a complex net, first, the noise sources have to be identified. Assuming that different noise sources are uncorrelated, their power adds in the noise power of the output signal. The following noise sources are considered: the input current and voltage noise of the preamplifier, the Johnson noise of the load resistor R_L, the shot and excess noise of the APD current, and the noise of the second and third amplifiers.

First, a rough estimation of the signal levels was done and the contribution of the amplifier input current noise was compared to the shot noise from the detector. At the lowest expected photon flux ($10^9\ \mathrm{s}^{-1}$), the APD output current is in the 10 nA range, the photon statistical noise (without APD excess noise) is around 100 pA for 1 MHz bandwidth. The

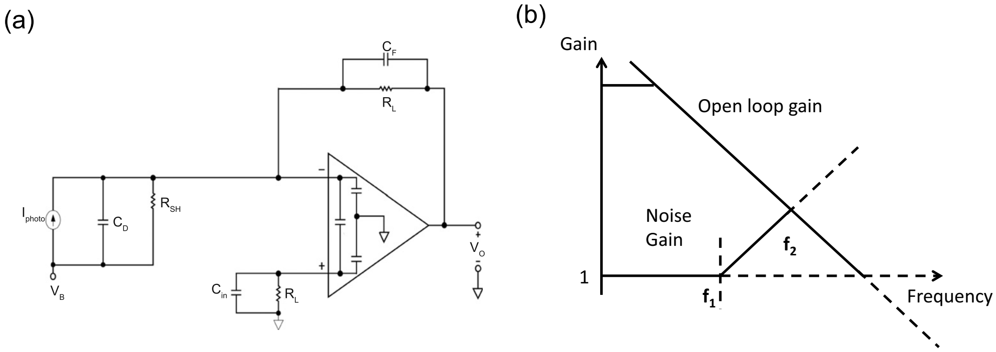

FIG. 2. Model of the preamp electric circuit (a) and the noise peaking effect (b).

amplifier input current noise for the same bandwidth is less than 1 pA; therefore, it can be completely neglected, even for a PPD, where the current noise is 10 pA.

To analyze the effect of the other preamplifier noise sources, an equivalent scheme of the preamplifier and APD is presented together with its frequency response in Fig. 2. The noise gain and the signal gain have to be distinguished and analyzed as a function of frequency. For the signal gain, only the photocurrent generator (I_{photo}) and the feedback components (R_L, C_F) are considered, which define a constant gain current to voltage converter up to the frequency $f_2 = 1/2\pi C_F R_L$. As was already mentioned, the intrinsic gain of APD is not noiseless. The amplitude of the output noise of the preamplifier due to the APD current noise can be described as

$$N_{\mathrm{shot}} = \sqrt{2qI_{\mathrm{photo}}M^2FB} \cdot R_L, \tag{1}$$

where R_L is the load resistor, M is the applied APD gain, q is the electron charge, and $I_{\mathrm{photo}} = q \cdot N \cdot \mathrm{QE}$ is the photocurrent at $M=1$ given by the incoming number of photons per second (N) and the QE. For the calculation below, QE=0.85 is used. F is the excess noise factor, which gives the additional noise generated by the avalanche process,

$$F = M^x. \tag{2}$$

Here, x is the excess noise index. The excess noise is caused partly by the statistical nature of the avalanches, partly by the random location of the photoelectron production in the absorption layer. The latter is wavelength dependent; therefore, the excess noise is wavelength dependent as well. The present calculation is limited to a fixed wavelength where $x = 0.3$,[10] resulting to $F = 3.2$ excess noise factor for $M = 50$ gain, which is common in our applications.

The effect of the input voltage noise of the preamplifier on its output signal is determined by the noise gain. Its frequency dependence is shown in Fig. 2(b). Up to frequency f_1, the noise gain is unity, where $f_1 = 1/2\pi C_{\mathrm{in}} R_L$, where $C_{\mathrm{in}} = C_D + C_F$. Between f_1 and f_2, the noise gain increases with frequency linearly on a log-log scale up to C_{in}/C_F. From here, the noise gain is constant, but this is cut by the filtering of the following stages. The contribution of the amplifier input voltage noise to its output noise, limited to the bandwidth of the whole system, can be approximated as

$$N_{\mathrm{voltage}} = N_{f_1} + N_{f_2}, \tag{3}$$

$$N_{f_1} = VEN \cdot \sqrt{f_1}, \tag{4}$$

$$N_{f_2} = VEN \cdot \sqrt{\frac{C_{\mathrm{in}}}{C_F}} \cdot \sqrt{f_1 - f_2}. \tag{5}$$

In the design of the experiment, there is a trade-off between the optical requirements needing a large surface detector and the SNR considerations desiring the minimum surface since the capacitance of a photodiode scales with its surface. In the typical optical realization, the detector size would vary between 1 and 5 mm, resulting in typical capacitance between 3 and 100 pf. The feedback capacitance C_F sets the bandwidth of the circuit and also stabilizes the amplifier.

The load resistor (R_L) Johnson noise is given by

$$N_{\mathrm{Johnson}} = \sqrt{2 \cdot 4kTR_LB}, \tag{6}$$

where k is Boltzmann's constant and T is the absolute temperature. The factor of 2 comes from two R_L from both inputs of the preamp (Fig. 1).

The noise of the second and the third stages were proved to be negligible compared to the abovementioned noise sources; therefore, they are not taken into account. The more detailed theory of the noise gain can be found in Refs. 9 and 10; only the main results relevant for this application were recalled in this paper.

The above noise sources (APD current noise, R_L Johnson noise, and amplifier voltage noise) and the amplification process were calculated numerically. On the basis of this calculation, three parameters (M, R_L, and C_F) have to be selected to optimize the signal-to-noise ratio at a given photon flux and bandwidth. Although the calculations in some cases result in extremely low C_F, the practical lowest limit is a few picofarads for this value. In the following example, the optimal parameters of the amplifier built for TEXTOR are shown. In this case, large surface detectors were used, which also have high capacitance. In the calculation, the minimum capacitor value determines the maximum resistor as they define the desired bandwidth as well. From the experiments, this maximum pair is set to 68 kΩ and 4.7 pF; the bandwidth was set to 500 kHz and the achievable maximum APD gain is limited to 100, which is the value close to the breakdown limit. One has to note that the stability limit of the amplifier changes with the capacitance of the diode. The optimized parameters of the amplifier, the optimal noise to signal ratio, and the noise level of different noise sources are

TABLE I. Calculated noises and optimized gain for the TEXTOR amplifier for different photon flux.

Photon flux	Noise to signal ratio	Noise (mV)	Photonic noise N_{shot} (mV)	Resistor noise $N_{Johnson}$ (mV)	Applied gain
5×10^{7}	1.13	4.9	1.3	3.9	100
1×10^{8}	0.59	5.1	1.9	3.9	100
1×10^{9}	0.087	7.6	5.9	3.9	100
5×10^{9}	0.032	12.6	11.7	3.9	90
1×10^{10}	0.022	13.3	12.4	3.9	70
5×10^{10}	0.009	13.4	12.5	3.9	35

shown for different photon fluxes in Table I. The noise resulting from the preamplifier voltage noise is 2.6 mV, while from the current noise, we get 0.15 mV at amplifier gain 93, which was set at the TEXTOR system.

As one can see, there is an optimal gain, which is a trade-off between the signal amplitude and the APD excess noise. Practically in our recent low light level applications, R_L has to be set to a maximum available value that still could be stabilized at the requested bandwidth. If the light level increases, the photonic noise becomes dominant and the APD gain should be decreased, reducing the APD excess noise caused by the avalanche process. In real BES measurements, the light level can be different in various plasma scenarios and the background light level can also be very different. However, the APD voltage is not planned to be controlled real-time, as it would make the data analysis very difficult. It is worth noting that above 10^9 photon flux, the noise is limited by the photonic noise, which is not dependent on the temperature. Therefore, cooling of neither the load resistor nor the detector offers any advantage over room temperature operation.

Using the noise model of the electric circuit, we can compare the SNR of different detectors dependent on the incident light level at 1 MHz bandwidth. This comparison is shown in Fig. 3, showing the noise-to-signal curve of the ideal detector, a PMT, two APDs, and two PPD detectors. The ideal detector is the 100% QE detector where the amplification is noiseless. As a PMT, a multialkali cathode PMT was chosen because it has relatively high QE (10%) in the requested wavelength range. Due to the high intrinsic gain the noise of any read out electronics was neglected for the PMT. The noise curves of two different APDs are given: a smaller surface APD (3.14 mm^2, 11 pF) and a larger surface APD (25 mm^2, 80 pF). For the APD calculations, the optimized gain resulting from the maximum SNR was used, which means lower gain is applied at a higher photon flux. A large surface (5.7 mm^2, 65 pF) photodiode with the same read out electronics and the same circuit parameters that was used with large surface APD is also plotted. It has to be noted that for the calculations of the noise curves of the APD detectors and the large surface PPD detector, room temperature was assumed.

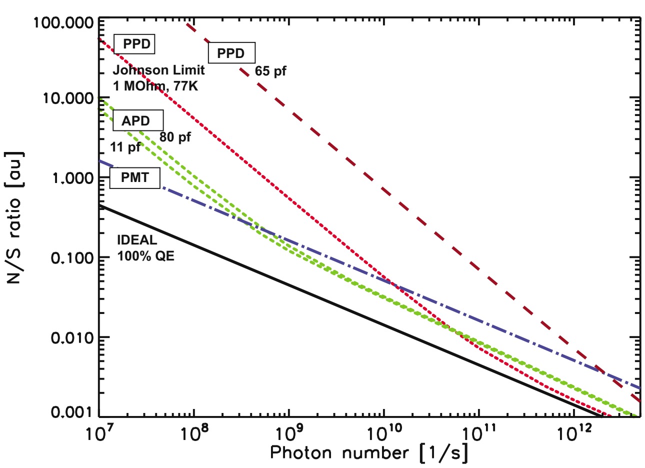

FIG. 3. (Color online) Comparison of the noise to signal ratios of different detectors as a function of incident light level at 1 MHz bandwidth. The optimal APD gain is applied for each photon flux.

To complete the picture, the achievable limit of the PPD SNR is estimated. In the case of PPD, the largest resistor value is desirable as the signal level grows linearly with this value and the Johnson noise changes as square root. The electrical components always have some parasitic capacitance, so for a 1 MHz bandwidth, we chose 1 MΩ as an upper limit for the feedback resistor (that means 0.16 pF feedback capacitance). The performance of the detector can be optimized using cryogenic cooling as the Johnson noise scales with square root of the temperature, as shown in Eq. (6). The reduction of the noise using cryogenic temperature was also shown experimentally.[11] To estimate the limit of this technique, the amplifier noise was neglected and noise is calculated as the sum of the photonic noise and Johnson noise. Although this assumption underestimates the noise, as in a high frequency PPD system the voltage noise can dominate the Johnson noise,[12] it represents the achievable physical limit.

From this figure, the following can be deduced: at low light level, the PMTs are still the optimal choice. APDs should be considered above a photon rate of few times 10^8 photons/s at 1 MHz bandwidth. There is a two order of magnitude wide gap in the incident photon flux ($\approx 5\times10^{8}-5\times10^{10}$ photons/s at 1 MHz) where APDs are superior to both PMTs and optimized small PPDs. Larger photodiodes should only be used at even higher photon flux above $\approx 10^{13}$ photons/s.

The photon flux values, where one detector type becomes superior, are strongly dependent on the required bandwidth. The photon flux range where the APD detector is the optimal choice widens with higher bandwidth. It is also noted here that large area detectors are optimal for large solid angle collection optics, as large demagnification cannot be

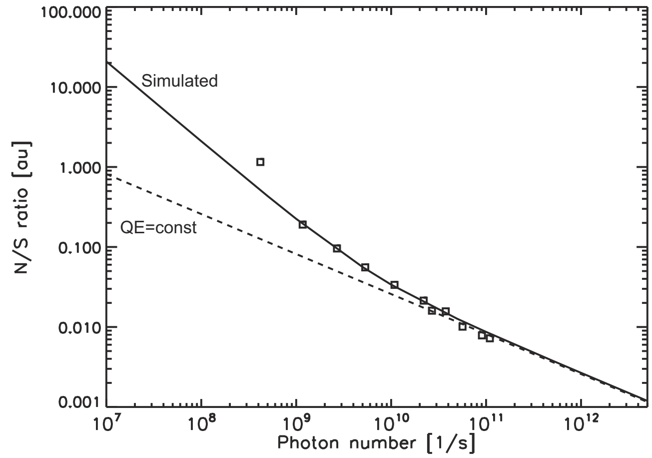

FIG. 4. The APD based detector circuit performance test against the theoretical model shown by the solid curve.

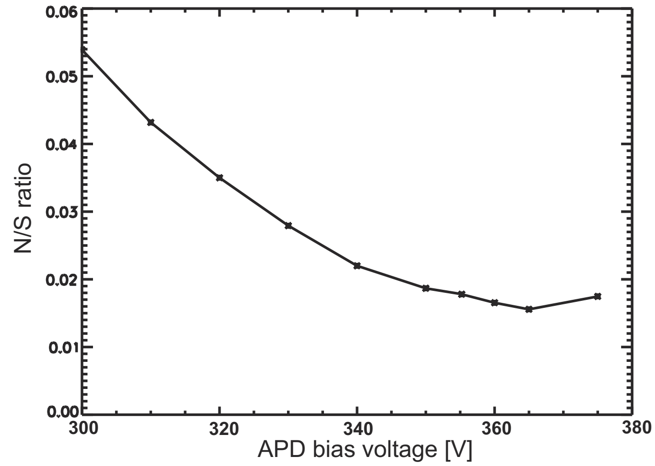

FIG. 5. The measured NSR vs the applied voltage at 2.7×10 photons/s incoming flux.

achieved without the loss of light. In this case, the photon flux range, where APDs are the optimal choice, grows to three to four orders of magnitude.

An additional optimization of the SNR can be introduced by increasing the feedback resistor of the first stage at the expense of lower bandwidth. This will attenuate the high frequency transmission, which can be compensated for, to some extent, either electronically in the second stage[5] or digitally during postprocessing. This technique can be used both in the case of the PPD and the APD detectors. As described above, increasing the feedback resistor improves SNR as $\sqrt{R_L}$ (Johnson noise limited case) or R_L (voltage noise limited case). This will shift the knee of the APD and the PPD curves to the left in Fig. 3. However, there will always be a photon flux window where the APD is optimal. It has to be noted that this technique has no effect in the photon noise limited range, right to the knee of the curves.

As shown above, the crossover point of the noise curves of the PPD and APD detectors is a sensitive function of the bandwidth, the photon flux, and the detector size; therefore, a careful analysis is needed in each individual case. At the parameter combination of the upgraded DIII-D BES system,[12] the cryogenically cooled PPD detector with the above described frequency, compensation technique was found to be superior.

The first detector unit developed was the eight-channel APD system built for the MAST trial BES experiment[13] using large surface APD (25 mm^2, 80 pF) detectors and 1 MHz bandwidth amplifiers. The APD detectors are placed in a temperature stabilized housing. This unit was absolutely calibrated at the Hungarian National Office of Measures with a calibrated stabilized laser source, attenuated by calibrated filters. In a series of measurements, the NSR of the signal as a function of incident light level was examined and plotted against the calculated values in Fig. 4. The experiment and the calculations showed good agreement, except at the lowest light level where measurement was made difficult by the low signal level.

The SNR of the detector was also examined as a function of the applied bias voltage, hence changing the gain. An optimum bias voltage is predicted at sufficiently high photon flux. At 2.7×10 photons/s incoming photon flux, the NSR minimum is shown in Fig. 5

It has to be mentioned that the gain as a function of voltage can have a large scatter from detector to detector; therefore, the voltage should ideally be set for each channel individually. Because of the noise peaking effect, the power spectrum of the measured signal is not flat. This effect can be either solved electronically by applying a frequency compensating stage or by applying a numerical compensation. Additionally, by applying a higher sampling frequency, the bandwidth can be set more precisely in the digital solution.

V. FIRST APPLICATIONS OF THE NEW DETECTOR IN BES SYSTEMS

Some illustrative measurements are shown from the trial BES system from MAST (Ref. 13) and the Li BES system from TEXTOR.[14] The selection of the detector and electronics design was strongly influenced by the constraints from the optics. For both experimental setups, large surface detectors had to be used where the sensitive area of adjacent detectors is very close to each other with the smallest possible gap. Due to this requirement, the Hamamatsu S8664-55 APD was chosen. This has 5×5 mm^2 active surface, QE of $\sim$0.85, and photosensitivity of 20 A/W at the desired wavelength using $\sim$360 V bias voltage. It is mounted on a rectangular ceramics housing that defines the detector outer dimension at 9×10.6 mm^2. Details of the MAST BES results have been published separately.[13] In the first series of the measurement, the bandwidth was set to 1 MHz. The measured signal level varies between 20 and 80 mV as the beam emissivity changes, which means 5×10^9 photons/s at the maximum of the light profile. One has to note that the trial system is a piggy-back experiment on the charge exchange measurement and is not optimized for turbulence measurements. The main aim was to test the detectors and the simulation codes to build a proper 2D BES system for the plasma core. The dominant noise source is the electronic noise of the preamplifier, so the S/N increases linearly with the signal level. Although the S/N is quite low (2.5–10), using a corre-

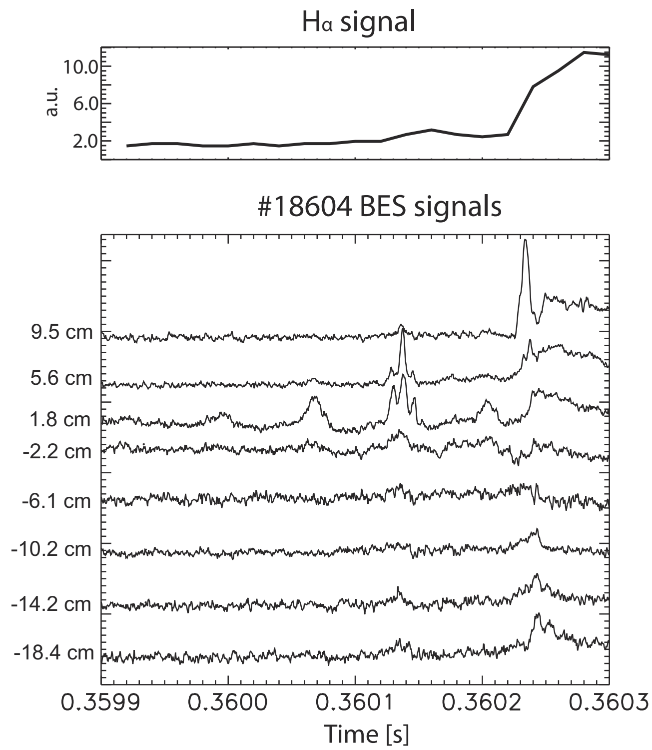

FIG. 6. Precursor oscillations preceding an ELM in an L-SND configuration at MAST. The numbers near the vertical axis show the measurement location relative to the separatrix.

lation technique, the edge turbulence could be resolved with percentage precision. The high temporal resolution makes it possible to examine fast transient events. As a remarkable example, edge localized mode (ELM) precursor oscillations were observed in the pedestal region of neutral beam injection (NBI) heated H-mode discharges with a lower single null divertor (L-SND) magnetic configuration, as shown in Fig. 6.[15] After these successful measurements, the development of the 2D BES system has started. A compact 2D camera is being developed, utilizing a 2D APD array with 4×8 channels. The expected photon flux of few times 10^{11} photons/s would result in SNR of 125–330, allowing direct fluctuation measurement down to a few tenths of a percent.[13]

A beam emission spectroscopy diagnostics system optimized for density turbulence measurements has been recently installed at the TEXTOR tokamak.[16] A 16-channel APD detector unit was built using the same detectors as on MAST. In this application, the detector unit is installed close the device and beam light is directly imaged to the detector row, avoiding the losses from coupling the light to the fibers. By building a row of detectors, one can implement a 5 mm wide sensitive stripe with a fill factor of around 50%. Depending on the actual optical setup, the fill factor can be improved by small individual optics, as was implemented in the observation system of TEXTOR BES. The beam emission is measured in 500 kHz analog bandwidth with 2.5 MHz sampling. Individual lenses are installed to increase the fill factor to nearly 100%. The 16 cm radial coverage extends from the scrape off layer (SOL) into the edge plasma to $r/a=0.85$. The photon flux at the maximum of the emission profile is up to 3×10^{10} (photons s^{-1})/channel causing 2% photon statistical noise in the signal, including the excess noise of the APD amplification process. At this signal level, the photonic noise exceeds other noise sources of the amplifier and the measurement of plasma density fluctuations becomes possible over the whole radial range. This is even true at $r/a<0.9$, where the fluctuation level drops below 1%, as correlation techniques are sensitive down to the 0.1% level in light fluctuations.

In the SOL, the amplitudes are higher (in the 10% range) but measurement is complicated by a relatively large background light level originating from the limiter in the background. A fast beam chopper system has been developed for this situation where the beam can be switched on and off with up to 250 kHz frequency. This is higher than the background light fluctuation frequency caused by SOL turbulence; therefore, the beam light can be corrected for the background. The upgraded Li beam diagnostics, which is a combination of the advanced beam manipulation system and the optimized optics and detectors, will be published in a separate paper.[14]

As an example, power spectra from a core channel and a SOL channel are shown in Fig. 7. The difference between the SOL and the edge channels is clearly seen; SOL fluctuations are at lower frequency and higher amplitude. The spectra of the calibration light source are flat with a bandwidth of 500 kHz. The noise peaking effect is clearly seen in the spectra without light, as described in the previous sections.

The silicon based APD detectors are sensitive to neutron and gamma radiation. At TEXTOR, the APD detectors are installed close to device, ≈ 1 m from the vacuum chamber. The effect of the neutron and/or gamma is seen as large instantaneous peaks in the signal, caused by the large electron avalanche. At TEXTOR, even in the case of deuterium beam heated deuterium plasma, these peaks were statistically insignificant. One has to note here that for larger devices, this effect is not negligible and sufficient neutron and gamma shielding is necessary. In the case of MAST 2D BES, the setup was designed to allow the installation of a shield, which might be necessary with MAST Upgrade. There is another effect of the high energy radiation on silicon detectors; permanent channels can be formed increasing the black current. In our case, no significant changes were seen in the APD performance after 2 yr of operation.

Finally, at JET, a four-channel trial system was installed on the Li beam diagnostics in 2008. In this experiment, the light is coupled into 1 mm diameter optical fibers. From the output of the fiber, light rays are made parallel by a lens and filtered with an interference filter and the light is imaged onto a Hamamatsu *S*8664-20*k* 2 mm diameter APD detector. The amplifiers were set to 500 kHz bandwidth $R_L=68\ \mathrm{k}\Omega$, $C_F=4.7$ pF. The noise peaking effect is not significant. Although the light level was very poor in these measurements ($<10^9$ photons/s), the basic turbulence properties could be determined using longer integration time of the correlation functions.

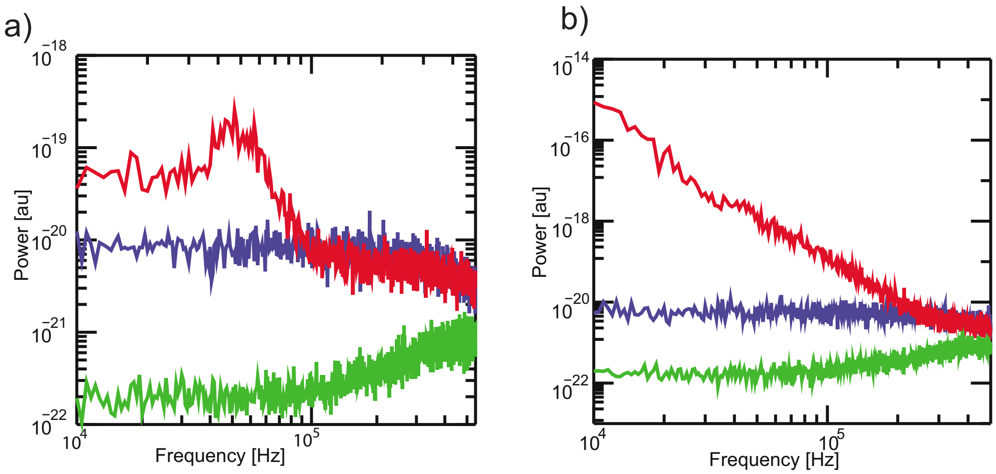

FIG. 7. (Color online) Power spectra of TEXTOR Li BES signals in the edge plasma (a) and in the SOL plasma (b). The lowest curves on both figures (green online) were measured without incident light. The middle curves (blue online) were measured with calibration light source, and the upper curves (red online) with plasma. The calibration light intensity was selected in a way that the signal mean level was identical to the corresponding plasma signal.

VI. CONCLUSIONS AND OUTLOOK

An APD based detector has been developed for high frequency low level light measurements for visible wavelength range. These detectors are recently used in fusion plasma physics diagnostics but could be used elsewhere as well. The avalanche photodiode has an advantage of large quantum efficiency over the PMT and also has an additional internal gain. This gain makes the APD detector a better choice over the normal photodiodes (PPD) in a certain photon flux range around $\approx 5\times10^{8}$–5×10^{10} photons/s at 1 MHz bandwidth. This range depends on the desired bandwidth and actual detector parameters. A state-of-the-art readout electronics was designed and built for APD detectors. The noise level was extensively investigated by model calculations and measurements. The theoretical model has excellent agreement with the experiments. Based on this experience, APD detector units were built and installed on the MAST, TEXTOR, and JET BES diagnostics. First measurements showed results in agreement with the expectations.

ACKNOWLEDGMENTS

This work, supported by the European Communities under the contract of Association between EURATOM and the Hungarian Academy of Sciences, was carried out within the framework of the European Fusion Development Agreement. The views and opinions expressed herein do not necessarily reflect those of the European Commission.

[1] B. Schweer, Fusion Science and Technology **45**, 434 (2004).
[2] G. McKee, R. Ashley, R. Durst, R. Fonck, M. Jakubowski, K. Tritz, K. Burrell, C. Greenfield, and J. Robinson, Rev. Sci. Instrum. **70**, 913 (1999).
[3] S. Zoletnik, G. Petravich, A. Bencze, M. Berta, S. Fiedler, K. McCormick, and J. Schweinzer, Rev. Sci. Instrum. **76**, 073504 (2005).
[4] S. Zoletnik, M. Anton, M. Endler, S. Fiedler, M. Hirsch, K. McCormick, and J. Schweinzer, Phys. Plasmas **6**, 4239 (1999).
[5] R. J. Fonck, R. Ashley, and R. Durst, Rev. Sci. Instrum. **63**, 4924 (1992).
[6] G. K. McCormick, S. Fiedler, G. Kocsis, J. Schweinzer, and S. Zoletnik, Fusion Eng. Des. **34–35**, 125 (1996).
[7] R. Fischer, E. Wolfrum, and J. Schweinzer, Plasma Phys. Controlled Fusion **50**, 085009 (2008).
[8] T. Oishi, S. Tanaka, S. Kado, M. Yoshinuma, and K. Ida, Rev. Sci. Instrum. **75**, 4118 (2004).
[9] Analog Devices AD8065 datasheet.
[10] Hamamatsu Photodiode Technical Information.
[11] G. R. McKee, R. J. Fonck, D. K. Gupta, D. J. Schlossberg, M. W. Shafer, and R. L. Boivin, Rev. Sci. Instrum. **77**, 10F104 (2006).
[12] D. K. Gupta, R. J. Fonck, G. R. McKee, D. J. Schlossberg, and M. W. Shafer, Rev. Sci. Instrum. **75**, 3493 (2004).
[13] A. R. Field, D. Dunai, N. J. Conway, S. Zoletnik, and J. Sárközi, Rev. Sci. Instrum. **80**, 073503 (2009).
[14] G. Petravich, G. Anda, D. Dunai, S. Zoletnik, and J. Sárközi, Rev. Sci. Instrum. (unpublished).
[15] S. Zoletnik, D. Dunai, A. R. Field, and A. Kirk, Proceedings of the 35th EPS Conference on Plasma Physics, 2008, ECA Vol. 32D O-4.031.
[16] D. Dunai, S. Zoletnik, G. Anda, and G. Petravich, Proceedings of the 36th EPS Conference on Plasma Physics, 2009, ECA Vol. 33E P-1.182.